THE ASTROPHYSICAL JOURNAL, 492:833–842, 1998 January 10

RADIATIVE ACCELERATIONS FOR EVOLUTIONARY MODEL CALCULATIONS

J. RICHER[1] AND G. MICHAUD[1]
Département de Physique, Université de Montréal, Montréal H3C 3J7, Canada
F. ROGERS AND C. IGLESIAS
Lawrence Livermore National Laboratory, PO Box 808, Livermore, CA 94550
S. TURCOTTE[1]
Département de Physique, Université de Montréal, Montréal H3C 3J7, Canada
AND
F. LEBLANC
Département de Physique, Université de Moncton, Moncton E1A 3E9, Canada
Received 1997 March 10; accepted 1997 August 21

ABSTRACT

Monochromatic opacities from the OPAL database have been used to calculate radiative accelerations for the 21 included chemical species. The 10^4 frequencies used are sufficient to calculate the radiative accelerations of many elements for $T > 10^5$ K, using frequency sampling. This temperature limit is higher for less abundant elements.

As the abundances of Fe, He, or O are varied, the radiative acceleration of other elements changes, since abundant elements modify the frequency dependence of the radiative flux and the Rosseland opacity. Accurate radiative accelerations for a given element can only be obtained by allowing the abundances of the species that contribute most to the Rosseland opacity to vary during the evolution and recalculating the radiative accelerations and the Rosseland opacity during the evolution.

There are physical phenomena that cannot be included in the calculations if one uses only the OPAL data. For instance, one should correct for the momentum given to the electron in a photoionization. Such effects are evaluated using atomic data from Opacity Project, and correction factors are given.

Subject headings: atomic data — diffusion — stars: interiors

1. RADIATIVE ACCELERATIONS AND STELLAR EVOLUTION

Standard stellar evolution assumes that there is no particle transport outside convection zones. However, as a minimal process, atomic diffusion is necessarily present. Transport by atomic diffusion mainly involves a competition between gravity and radiative acceleration (Michaud 1970). The recent availability of large atomic databanks has made it possible to calculate radiative accelerations for all elements contributing substantially to the Rosseland opacity. It is the aim of this paper to show how the OPAL data (Rogers & Iglesias 1992a, 1992b; Iglesias & Rogers 1995, 1996) can be used in such calculations and to investigate the limitations of the existing databanks. Detailed stellar evolution models are presently being calculated using the opacities and radiative accelerations presented here (Turcotte et al. 1998b).

The importance of radiative accelerations arises from the fact that they dominate atomic diffusion in many stars (Vauclair & Vauclair 1982). They clearly dominate in the external regions of all main-sequence stars with $T_{\rm eff} > 6000$ K (Michaud et al. 1976), of horizontal branch stars with $T_{\rm eff} > 8000$ K (Michaud, Vauclair, & Vauclair 1983), and of the hottest white dwarfs (Chayer, Fortaine, & Wesemael 1995). Competing hydrodynamic processes (e.g., turbulence or mass loss) may moderate the expected effects of atomic diffusion and radiative acceleration even in the radiatively stable regions of stellar interiors; such processes were ignored in this study.

The relatively large contribution of iron to the Rosseland opacity in main-sequence stars implies that iron can be pushed upward, become overabundant, and modify the stellar structure through the averaged opacity. The extent to which this is possible can only be evaluated by using accurate radiative accelerations in detailed stellar evolution calculations. Since one modifies the other, the Rosseland opacity and the radiative accelerations should ideally be calculated with the same atomic data to assure compatibility.

Close to the stellar center, the L_r/M_r ratio increases, since nuclear reactions mainly occur in a small central core. This may lead to an increase of the relative importance of radiative acceleration ($\propto L_r$) compared to gravity ($\propto M_r$). Radiative accelerations have never been evaluated there.

To calculate the direct effect of the radiation pressure gradient on stellar structure, one only needs the information required to calculate opacities. However, radiation pressure also modifies stellar evolution through atomic diffusion. For the diffusion of atomic species, one needs differential radiative accelerations, that is, the radiative acceleration felt by an individual atomic species through the absorption of a photon and before the momentum change is shared, through collisions, with the other species of the gas. This requires more information than is needed to calculate opacities (Gonzalez et al. 1995b, hereafter GLAM; Seaton 1997). One needs to evaluate not only the absorption and scatter of photons but also how the momentum of photons is distributed among species and states of ionization, since this modifies the distribution in the rest of the gas. One must know how the momentum is shared between the electron and the ion after photoionization; this determines

[1] CERCA, 5160 Blvd Décarie, Montréal H3X 2H9, Canada.

whether the ion is pushed forward or backward by the photon. One must also determine whether an He atom, for instance, remains neutral or ionizes after absorption in a line, since that determines how rapidly the momentum gained by He is shared with the whole gas (GLAM).

In the next section, we present the radiative accelerations that follow from the OPAL monochromatic spectra. Only information contained in the OPAL database will be used. For stellar evolution calculations, they allow one to determine the time evolution of abundances and the competition for photons among the various species. The density of the frequency grid will, however, be seen to be insufficient to calculate the radiative accelerations of some elements in the outer regions of stellar envelopes. For those cases requiring a higher density grid than is available (an increase in frequency resolution by as much as a factor of 100 may be necessary in some cases to reach $\sim 1\%$ accuracy), an alternate approach is proposed in the following section, along with an evaluation of the importance of the corrections discussed in GLAM. This involves using OP atomic data (Seaton et al. 1994) to evaluate collision rates of individual transitions. Finally, examples of radiative accelerations in stellar models calculated taking the diffusion of some 30 species (the 21 element OPAL mix, ^{3}He, ^{13}C, and isotopes of LiBeB), their radiative acceleration, and their effect on the structure (Turcotte et al. 1998a, 1998b) will be briefly presented and analyzed.

2. RADIATIVE ACCELERATIONS ON THE OPAL GRID

In a first approximation, the radiative accelerations may be calculated using the fraction of the momentum flux that each element absorbs,

$$g_R(A) = \frac{1}{4\pi r^2}\,\frac{L_r^{\rm rad}}{c}\,\frac{\kappa_R}{X_A}\int_0^\infty \frac{\kappa_u(A)}{\kappa_u({\rm total})}\,\mathscr{P}(u)du\ . \qquad (1)$$

Here, u is the dimensionless frequency variable

$$u \equiv \frac{h\nu}{kT}\ , \qquad (2)$$

$\mathscr{P}(u)$ is the *normalized* blackbody flux,[2] given by

$$\mathscr{P}(u) \equiv \frac{15}{4\pi^4}\,\frac{u^4 e^u}{(e^u-1)^2}\ , \qquad (3)$$

and $L_r^{\rm rad}/(4\pi r^2 c)$ is the total radiative momentum flux at radius r. Within stellar models, this factor varies as $1/r^2$ from the surface down to the region where energy is generated. This variation is the same as that of local gravity except near the center, since energy generation is more concentrated than mass. Note that abundance changes modify g_R both through κ_R and through the integral given in equation (1). Within convection zones, a fraction of the energy flux is carried by convective motions, and the luminosity $L_r^{\rm rad}$ in equation (1) then represents only a fraction of the total luminosity. The g_R were calculated for the 21 abundance solar mix given in Table 1.

The radiative accelerations are always calculated at the (T, R) grid points of OPAL [where $R \equiv \rho/(T/10^6)^3$], the interpolations between grid points being made after the radiative acceleration calculations.[3] Figure 1 shows g_R calculated from the OPAL data by a direct integration of equation (1) over the variable u, defined by equation (2). The detailed OPAL monochromatic opacities, $\kappa_u(A)$, of each atomic species were used to compute the total opacity κ_u(total) (which also includes electronic scattering). Results are shown as a function of T for the 21 elements included in the OPAL calculations at $\log R = -3$, which is typical of the density of stellar interiors for stars with $T_{\rm eff} \simeq 10000$ K. The factor $L_r^{\rm rad}/(4\pi r^2 c)$ is here replaced by its value at the surface of a star with $T_{\rm eff} = 10000$ K. The values of g_R are shown for solar abundances of all elements (*solid line*) and for an underabundance by a factor of 1/10. The κ_R is also shown in the lower right hand corner.

TABLE 1

STANDARD 21 ELEMENT MIX

Element	Mass Fraction	Number Fraction
H	7.000×10^{-1}	9.071×10^{-1}
He	2.800×10^{-1}	9.137×10^{-2}
C	3.466×10^{-3}	3.769×10^{-4}
N	1.063×10^{-3}	9.913×10^{-5}
O	9.645×10^{-3}	7.874×10^{-4}
Ne	1.973×10^{-3}	1.277×10^{-4}
Na	3.997×10^{-5}	2.271×10^{-6}
Mg	7.515×10^{-4}	4.038×10^{-5}
Al	6.476×10^{-5}	3.135×10^{-6}
Si	8.104×10^{-4}	3.769×10^{-5}
P	7.099×10^{-6}	2.994×10^{-7}
S	4.228×10^{-4}	1.723×10^{-5}
Cl	9.117×10^{-6}	3.359×10^{-7}
Ar	1.076×10^{-4}	3.517×10^{-6}
K	4.192×10^{-6}	1.400×10^{-7}
Ca	7.469×10^{-5}	2.434×10^{-6}
Ti	4.215×10^{-6}	1.149×10^{-7}
Cr	2.009×10^{-5}	5.047×10^{-7}
Mn	1.097×10^{-5}	2.607×10^{-7}
Fe	1.436×10^{-3}	3.358×10^{-5}
Ni	8.918×10^{-5}	1.984×10^{-6}

NOTE.— This is the standard 1996 OPAL mix for $Z = 0.02$, except for H and He, for which X(H) = 0.35 and X(He) = 0.63 in the original tables.

One first notes that the values of g_R are larger than $\log g \simeq 4$ for most elements over large temperature intervals, even for solar abundances. This will be discussed more precisely in § 4 for consistent stellar models in which the variations of g and g_R within the star will be included.

For Fe, the radiative accelerations for $T \leq 10^6$ K are large and could support more than the solar abundance. They are larger for the less-abundant other iron group elements.

For oxygen, the radiative acceleration is generally smaller than it is for Mn, Fe, or Si because of the larger solar abundance of oxygen, which causes more saturation, and the relatively small number of lines in the various ionization states of oxygen. For $T > 10^7$ K oxygen is completely ionized, so that its only contribution is through free-free absorption. Little is known about the way photon momentum is shared between ions and electrons during free-free absorption (see Massacrier & El-Murr, in preparation). In the present paper, the assumption is made that all momentum is absorbed by the ion. For $5 \times 10^5 < T < 5 \times 10^6$ K,

[2] In previous articles, the unnormalized function $P(u) \equiv u^4 e^u/(e^u-1)^2 \simeq 26\mathscr{P}(u)$ was often used (e.g. in Michaud et al. 1976 and GLAM).

[3] It would be inappropriate to interpolate spectra, since the relation between our independent variable u and ν is a function of T.

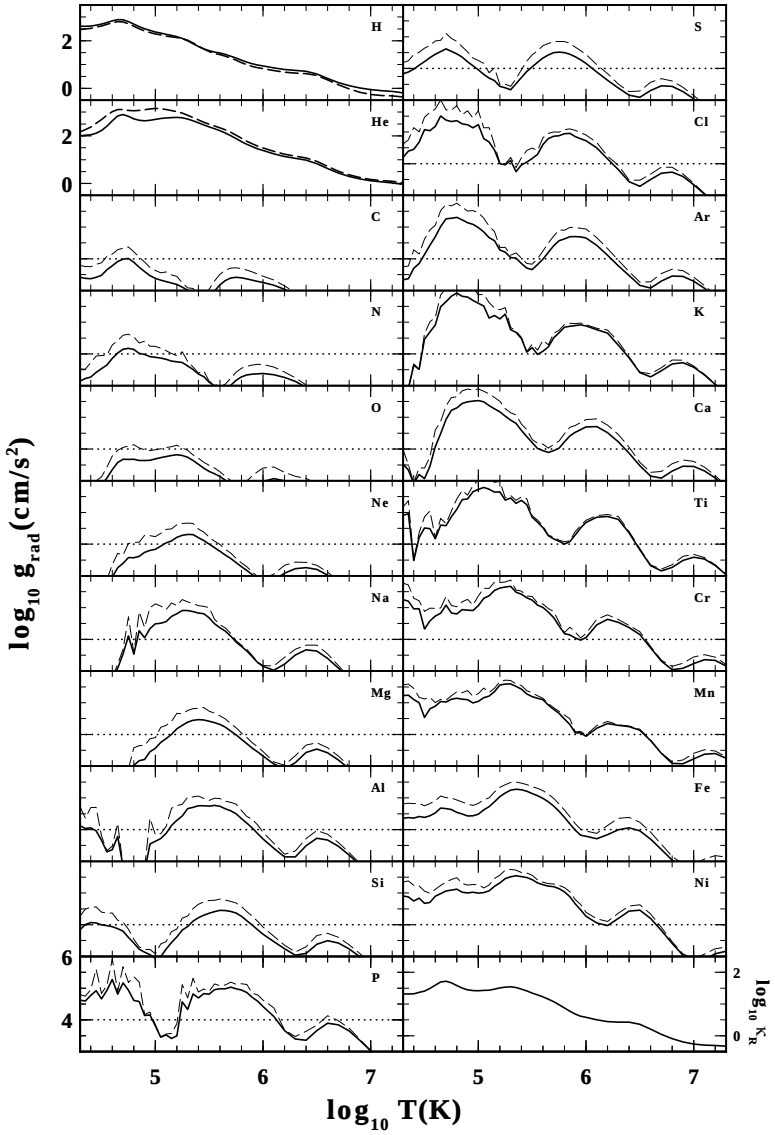

FIG. 1.—Radiative accelerations for all elements of the OPAL mix at our standard solar composition for log $R = -3$, $T_{\rm eff} = 10000$ K, and $L(r)$ independent of r. Except for H and He, the ordinate scale is the same for all elements and is given in the lower left corner panel. Solid line represents the acceleration at solar abundances. Dashed line represents the acceleration when the abundance by mass of the element is reduced by a factor of 10; others are unchanged except for renormalization of the whole. The Rosseland opacity for the composition of Table 1 is shown at the lower right.

the main contribution comes from hydrogenic oxygen. The same occurs at $3 \times 10^5 < T < 3 \times 10^6$ K for C. The lines are from hydrogenic configurations and are broadened by the linear Stark effect. Since only a small number of lines contribute, uncertainties in the broadening are reflected in uncertainties in the radiative accelerations. The radiative accelerations increase by a factor of up to 3 for a decrease in the abundance by a factor of 10. This depends on the degree of saturation of the lines, which depends on the broadening parameters.

In the OPAL tables, the contribution to electron scattering of electrons from the ionization of each element is part of that element's monochromatic opacities. This contribution should not be included in the numerator of equation (1) for radiative acceleration calculations, and has been subtracted from the monochromatic opacity used there. In practice, it is always much smaller than the ion contribution, and the subtraction does not significantly affect the results of diffusion calculations.

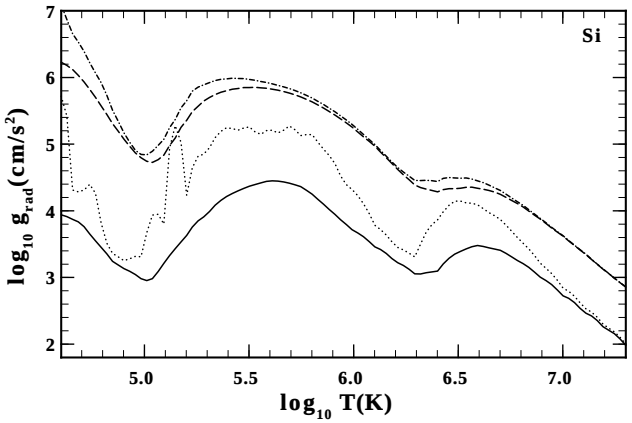

FIG. 2.—Radiative acceleration of Si at $T_{\rm eff} = 10000$ K. $X(\mathrm{H}) = 0.70$, $X(\mathrm{He}) = 0.28$. Solid line corresponds to log $R = -3$, $X(\mathrm{Si})_\odot$, dotted line corresponds to log $R = -3$, $X(\mathrm{Si})_\odot/1000$, dashed line corresponds to log $R = -1$, $X(\mathrm{Si})_\odot$, and dot-dashed line corresponds to log $R = -1$, $X(\mathrm{Si})_\odot/1000$.

Figure 2 shows the radiative acceleration of Si for the solar and the 10^{-3} solar abundance on the OPAL grid for $\log R = -3$ and -1. Most main-sequence stellar envelopes of interest have $\log R$ slightly larger than -3 but smaller than -2. The solar Si curve is relatively smooth, but the curve for underabundant Si shows large, apparently random fluctuations for $\log T \leq 5.7$. Fluctuations probably of the same origin can be seen in Figure 1 for Cr and most of the less-abundant species.

The main reason for those fluctuations can be seen in Figure 3. The sampling is clearly too coarse at $T \sim 2 \times 10^5$ K to reproduce individual line profiles. Approximating the line width by the Doppler width verifies that it becomes equal to the grid spacing only for $\log T > 7$ if the atomic mass number, A, equals 30. Progressing from one temperature grid point to the next, one may jump over a number of Doppler broadened lines. At larger density ($\log R = -1$), lines are more pressure broadened and the problem is relieved. Broad lines, such as presumably those of solar-abundance Si in Figure 2, are sufficiently sampled. These random fluctuations limit the temperature range over which radiative accelerations calculated using OPAL can be used. These limits depend on the abundances.

In the evaluation of equation (1) for Fe, it is the values shown in Figure 3*b* that matter. For the solar abundances used, Fe dominates the total opacity at the peak of some 25 to 30 lines [$\kappa_u(\mathrm{Fe})/\kappa_u(\mathrm{total}) > 0.5$] within the $u = 3.9$ to 4.0 interval. Dots show the value on the 10^4 point OPAL grid. Most lines are missed by the grid, but four are above 0.4 and contribute much more than an individual line should. The detailed line shape is clearly not reproduced, but it is sufficient to determine by sampling the fraction of the u interval over which the ratio of opacities becomes on the order of 1, where the integrand equals $\mathscr{P}(u)$. At those temperatures and abundances where Fe dominates the spectrum at a large fraction of the 10^4 frequencies of OPAL, the sampling is sufficient. However, this is much less true if the abundance of Fe decreases, since the number of frequencies where it dominates the spectrum then also decreases. Even if it has as many lines as iron, manganese has larger variations since, because of its smaller abundance, it dominates over a smaller fraction of the spectrum.

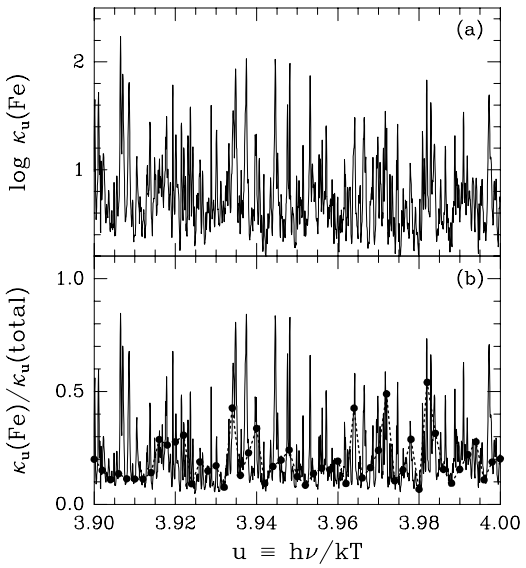

FIG. 3.—(*a*) Part of the OPAL Fe absorption spectrum at $kT = 20$ eV ($T \sim 2.3 \times 10^5$ K), and $N_e = 10^{19}$ cm^{-3}. The spectrum was computed at 4×10^5 frequencies uniformly covering the range $u = 020$. (*b*) Same spectrum divided by the total absorption spectrum of the standard 21 element mix (see Table 1). Absorption for elements other than Fe was interpolated from the 10^4 frequency OPAL tables; in that spectral region, the contribution from these elements is dominated by their continua. Dots represent the sampling subset at $\Delta u = 0.002$ resolution (10^4 frequencies) adopted by OPAL to compute their Rosseland mean opacity tables. Opacities are in cm^2 g^{-1}.

While large fluctuations clearly occur for individual Fe lines, on average, opacity sampling should give the correct radiative acceleration, as the following simple argument shows. Assume that one line of arbitrary shape is in an interval Δu of which it occupies only a small fraction. We are interested in evaluating its contribution to equation (1), that is, to an integral $\int f(u)du$. The function $f(u)$ is calculated at only one point, u_1, in the interval Δu, even though the line covers only a very small fraction of this interval. At that point, $f(u)$ is calculated exactly and opacity sampling approximates the integration over u by $f(u_1)\Delta u$. This can be much larger or smaller than the correct integral depending on where the line is with respect to u_1. If, however, we make a large number of such evaluations with points u_i chosen at random in the interval Δu, we can average them to obtain

$$g_R = \frac{1}{N} \sum_{i=1}^{N} f(u_i)\Delta u \, . \tag{4}$$

In the limit of large N, g_R approaches the correct value of the integral if the random values of $f(u_i)$ properly represent $f(u)$. This is the case if u_i is picked at random, uniformly, in the space over which one wishes to integrate. The opacity sampling method gives the right value of g_R if one calculates g_R many times and averages. A very large number of evaluations may be needed to represent a very peaked function covering only a small fraction of Δu.

Similarly, if a large number of lines contribute to a calculation of g_R, as for instance for Fe, calculating a large number of lines will be equivalent to sampling an interval many times, and the averaging process should lead to the right value. However, when only a limited number of lines contribute, variations either way are to be expected. On average, there is no reason to expect the evaluation to be higher or lower than the real value. If the fraction of Δu covered by lines of the element of interest is small, the variations are expected to be large, but not systematically either above or below the correct value.

Consequently, if one uses the OPAL data to calculate radiative accelerations for cases for which the sampling is not sufficient, we should not expect systematically erroneous results, but rather random fluctuations around the correct values.

2.1. *Competition for Photons between Elements*

The effect of a change in Fe and He abundances on the radiative accelerations of all other elements is shown in Figures 4 and 5. Solid lines in Figure 4 represent the ratio of the radiative acceleration for Fe abundance increased by a factor of 10 to the radiative acceleration for a solar Fe abundance [$g_R(A, 10x(\mathrm{Fe})_\odot)/g_R(A, X(\mathrm{Fe})_\odot)$]. Dashed lines show the same ratios when Fe is decreased, rather than increased, by a factor of $10[g_R(A, 0.1X(\mathrm{Fe})_\odot)/g_R(A, X(\mathrm{Fe})_\odot)]$. The corresponding Rosseland opacity ratios are also shown at the lower right of the figure.

It should be noted that increasing the Fe abundance by a factor of 10 increases the Rosseland opacity by a larger

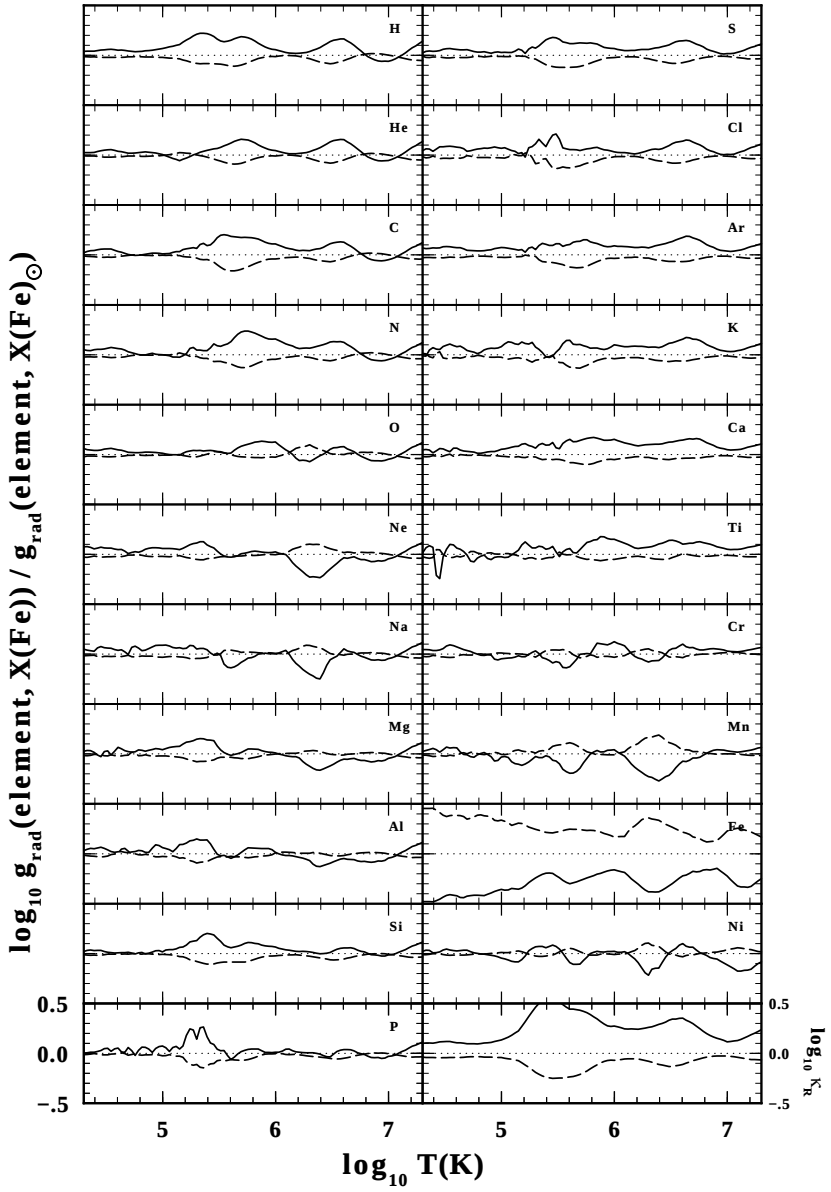

FIG. 4.—Ratios of radiative accelerations of various elements when Fe is 10 times overabundant (*solid line*) and 10 times underabundant (*dashed line*) to values when all abundances are solar. The only abundance that is changed is that of Fe, apart from an overall renormalization. All scales are given by P (*lower left corner*) except for the Rosseland mean opacity (*lower right corner*).

factor than that by which it modifies any of the radiative accelerations for $\log T > 5.2$. This modifies the stellar structure so that the effect of variations of Fe abundance on the radiative accelerations can only be obtained in evolutionary models where the effect of the increase of the Rosseland opacity is included. This will be briefly discussed in § 4. It is, however, instructive to see how large the effect is at given values of R and T.

The effect of the Fe abundance increase on g_R(Mn), for example, can be analyzed as arising from two phenomena. The increase in the averaged opacity appears in the numerator of equation (1), so that all radiative accelerations are proportional to that change. However, this effect is always partially cancelled by the competition for photons at the frequency where Mn absorbs (the factor $\kappa_u(A)/\kappa_u$(total) in eq. [1]). If increasing the Fe abundance increases the denominator at the frequencies at which the lines of Mn absorb, it then reduces the radiative flux absorbed by Mn. Depending on whether or not Mn has lines at the same frequency u as Fe, the g_R(Mn) will be either decreased or increased by the increase in the Fe abundance. In the case of Mn, at most values of T, an increase in Fe abundance decreases g_R(Mn). The effect is of the same order as, but always smaller than, the effect on g_R(Fe). However, depending on the element and on T, the effect can go either way. The increase reaches a factor of 1.8 for nitrogen, and the decrease a factor of 1.5 for nickel.

The effect on g_R of reducing the He abundance by a factor of 10 is shown in Figure 5. The radiative acceleration on He is increased by a factor of 3 for $\log T < 5.3$. At the same time, κ_R is *increased* by a factor 1.5, because the increased H abundance more than offsets the loss of He. Lowering the He abundance has an effect of a factor of 1.8 on the g_R for Mn, Cr, and C at $\log T = 5$, but a negligible effect on the g_R of Ti, S, or Na at the same T. Richer et al. (1997) have discovered that the reduction of the He abundance

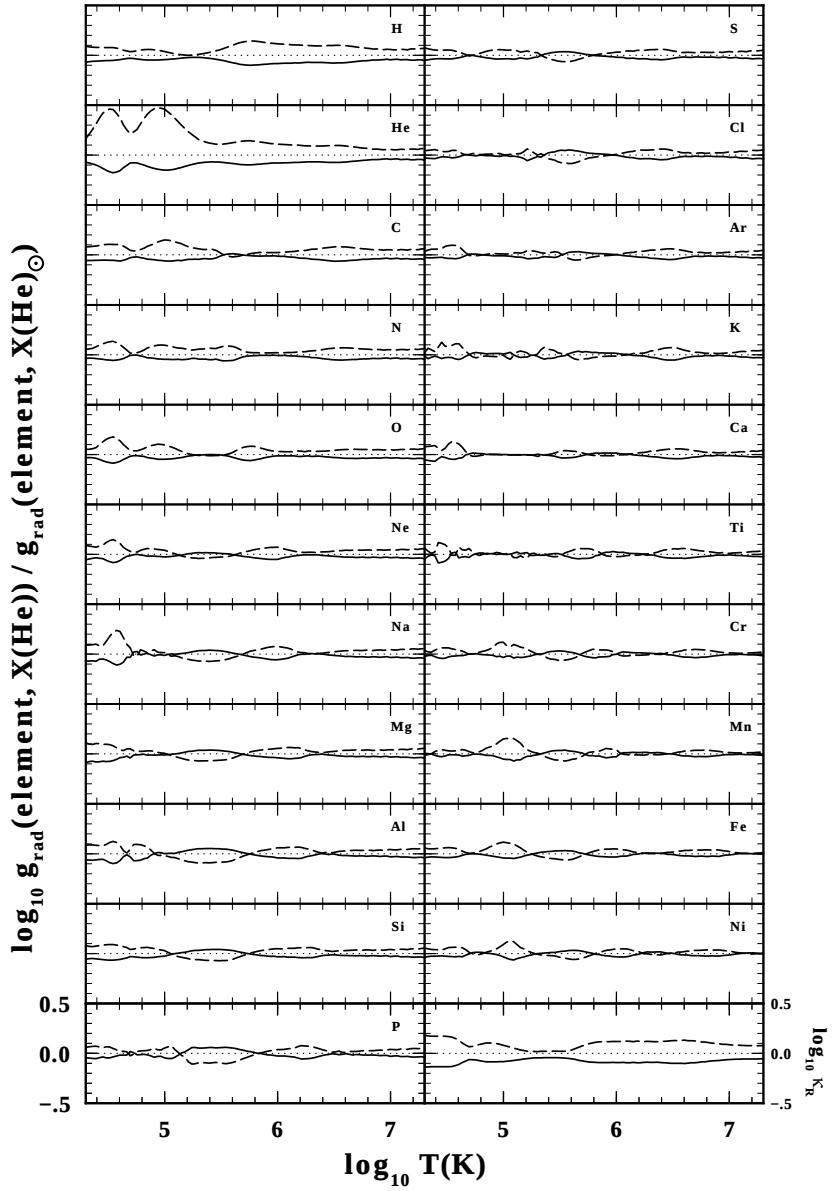

FIG. 5.—Ratios of radiative accelerations of various elements when He is overabundant by a factor of 2 (*solid line*) and 10 times underabundant (*dashed line*) to values when all abundances are solar. The only abundance that is changed is that of He, apart from an overall renormalization. All scales are given by *P* (*lower left corner*) except for the Rosseland mean opacity (*lower right corner*).

increases g_R(Li) by a factor of ~ 10. The effect on Li is larger because essentially only one line is important, and it occurs close to the maximum of the He continuum absorption.

3. DIFFERENTIAL RADIATIVE ACCELERATION AND ATOMIC PROCESSES

The calculations presented in the preceding section have two main limitations: (1) some physical processes important for *differential* radiative accelerations are not included and, (2) as described above, the opacity sampling misses some of the spectral features. These difficulties will be discussed in the next two subsections, along with solutions developed in GLAM.

3.1. *Atomic Processes*

We discuss successively the distribution of radiative acceleration among ions of a given species and the sharing of momentum between ion and electron following photoionization and free-free absorption.

3.1.1. *Averaging over Ions*

The importance of averaging over ions arises from the differences, among ions of a given species, in the collision probabilities for momentum exchange with the total gas. This implies that different diffusion coefficients should be applied to the momentum absorbed by different ions, for example, of He (Michaud et al. 1979). The situation is complicated by the relative timescales involved in the ionization and collision processes.

The atomic diffusion coefficient D_i and collision rate $\beta_{\mathrm{coll},i}$ of the ionization state i of element A are related by (Chapman & Cowling 1970)

$$D_i = \frac{kT}{m_A \beta_{\mathrm{coll},i}} . \tag{5}$$

The atomic diffusion coefficient of the neutral state of a species is some 100 times larger than that of the once-ionized state (Michaud, Martel, & Ratel 1978; GLAM). If

one weights the radiative accelerations by the diffusion coefficient, a photon absorbed in the neutral state is 100 times more efficient than if it had been absorbed in the once-ionized state. This can be important in outer stellar envelopes, especially for abundant elements whose lines are saturated. Between successive ionized states, the ratio is given approximately by $(Z+1)^2/Z^2$. Its importance decreases with increasing Z.

This simple argument assumes that the species remains in the same state of ionization until the momentum is shared with the other species, or implicitly that

$$\beta_{\mathrm{ion},i,j} \leq \beta_{\mathrm{coll},i}\ , \tag{6}$$

where i identifies the state of ionization and j the excitation state. In the ionization rates, the various ionization routes must be included. After a bound-bound transition, the ion is left in an excited state, j. It most often is repeatedly excited by collisions with electrons, with a rate $\beta_{\mathrm{exc},i,j}$, until it ionizes; this process makes the largest contribution to $\beta_{\mathrm{ion},i,j}$. The ratio $\beta_{\mathrm{ion},i,j}/\beta_{\mathrm{coll},i}$ then depends on j, the state of excitation in which the ion was left. Close to the ground state, the ion often deexcites before ionizing, and the ratio $\beta_{\mathrm{ion},i,j}/\beta_{\mathrm{coll},i}$ is often smaller than 1. For highly excited states, ionization is very rapid. Existing evaluations of this ratio are approximate and based on simple models of the excitation and ionization following photon absorption. GLAM and Gonzalez, Artu, & Michaud (1995a) compared excitation and deexcitation rates for CNO and concluded that the only states for which $\beta_{\mathrm{ion},i,j} \leq \beta_{\mathrm{coll},i}$ are those in which the principal quantum number $n \leq 2$. They consequently calculated radiative accelerations assuming that the momentum absorbed by bound-bound transitions ending on levels with $n = 2$ of ion Z was dissipated with the diffusion coefficient of ion Z, but that the momentum absorbed by transitions ending with $n \geq 3$ was dissipated by ion $Z+1$. For heavier metals, LeBlanc et al. (1995, 1998) calculated two sets of radiative accelerations (see also GLAM); these are used to obtain correction factors to the values of g_R calculated using OPAL data and are shown in Figure 6. In one set, they assumed that the momentum was dissipated in the same ionization state as that in which it was absorbed only if the bound-bound transition ends at a level with n one unit above the fundamental (*dashed line*), while in the other set the bound-bound transition must end in a level with the same n as the fundamental (*solid line*). Comparing the two shows that the correction due to the state of ionization is important only at relatively low T. In the next subsection, another effect, important at higher T, is discussed.

By comparing results for the two sets of calculations, it can be seen that a more precise evaluation of the ratio of collision to ionization rates is needed at $\log T < 5$ if an accuracy of 10% is to be achieved. This requires a simulation of all the excitation paths leading to ionization after photon absorption.

3.1.2. *Momentum Sharing between Ion and Electron*

A free electron, after photon interaction, usually shares the momentum of the photon with an ion. While the electron is emitted nearly isotropically, there is a correction term of order v/c, where v is the velocity of the electron and c that of light. At energies of interest in stars, the anisotropy is small, but it can have a large effect because of the $2c/v$ ratio between the momentum of the electron and that of the photon for a given energy.

In the case of photoionization, Sommerfeld & Schurr (1930) and Schurr (1930) obtained the required differential cross sections to the required accuracy for the lower shells of hydrogen ($n = 1, 2$). (See Massacrier 1996 for more historical details.) Seaton (1995) gave results for the $n = 2$ and 3 states, while Massacrier (1996) extended them to any state of an hydrogenic ion, and Massacrier & El-Murr (1996) considered He and Li-like configurations (for ions that can be approximated by one electron moving in a central potential). Using those cross sections, Richer et al. (1997)

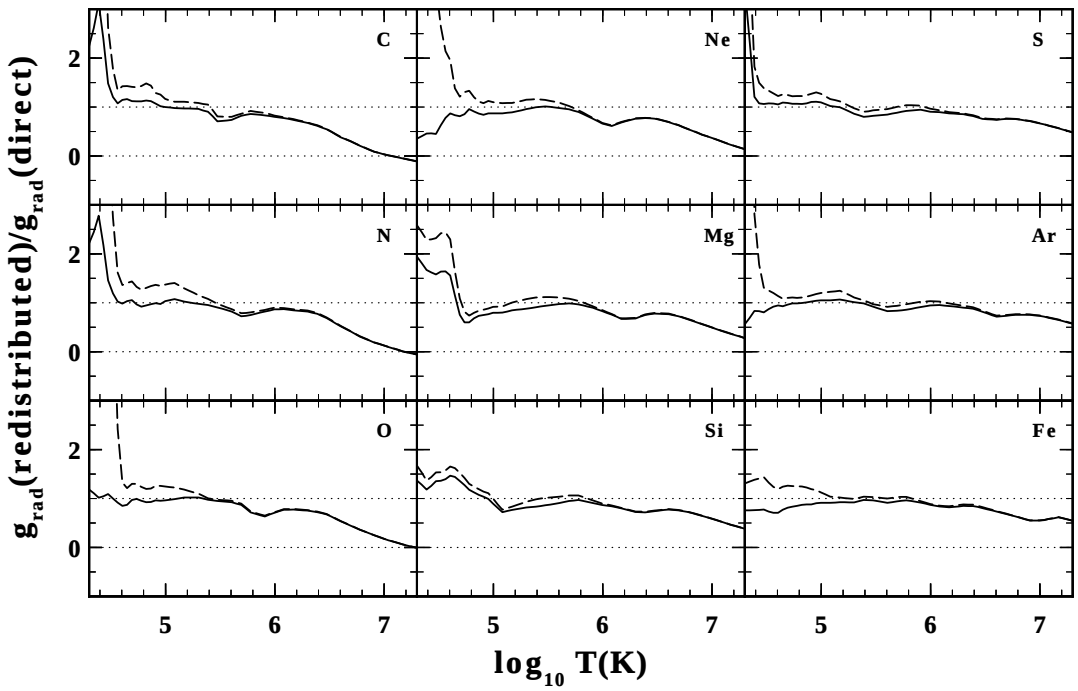

FIG. 6.—Corrections factors calculated using OP data at $\log R_e = 2.5$. The solid lines were calculated assuming $\Delta n = 0$, while the dashed lines assume $\Delta n \leq 1$. The correction factors include the effect of averaging over the ions, and of momentum sharing between ion and electron (see text for details).

showed that for any shell n of an hydrogenic ion, one could use the same simple formula for the effect of momentum sharing (see Michaud 1970):

$$f_{\rm ion}(n) = 1 - \frac{8}{5}\left(1 - \frac{\nu_n}{\nu}\right), \quad (7)$$

where $f_{\rm ion}$ is the fraction of the incident photon momentum that is carried away by the ion, and $h\nu_n$ is the ionization energy of the shell. These corrections have been included in the calculations of GLAM, and their effect is shown here in Figure 6.

The ratio of radiative accelerations calculated with the corrections mentioned above to those calculated without them is given for $\log R_e = 2.5$ ($\log R_e \equiv N_e/T^3$, in cgs units, N_e being the electron number density) as a function of T in Figure 6. The correction due to $f_{\rm ion}$ is largest at large T, while that due to the different states of ionization is largest at small T. The dashed lines give the correction factors calculated assuming that the momentum from absorption lines ending with a value of n equal to the fundamental plus 1 is spent in that state of ionization. The solid line was calculated assuming that only the momentum from lines ending with a value of n equal to that of the fundamental is spent with that state of ionization. For $T > 10^6$ K, electrons carry a significant fraction of the momentum. These correction factors are accurate for elements in hydrogenic configurations but not for those in other configurations. They are consequently accurate enough for CNO, Ne, Mg, Si, S, and Ar whenever these elements have correction factors significantly below 1 (for $T > 10^6$ K). But the correction factor is more uncertain for Fe, which is not in the hydrogenic state[4] even at $\log T = 7$.

3.2. *Opacity Sampling vs. Interval Averaging*

The approach of OPAL for evaluating opacities, and used here for g_R, involves calculating monochromatic opacities at fixed Δu intervals and using these values to integrate over u. This has the disadvantage described above for lines that can be entirely missed, or their contribution overestimated, when they are narrow.

The approach taken by GLAM is different and was motivated by the difficulties encountered by Michaud et al. (1979). Using the Los Alamos data then available, it was found to be impossible to calculate g_R for He because the frequency grid used to calculate opacities was too coarse. Instead, GLAM decided to separate the problem of calculating the line contributions to $g_R(A)$ into two parts. They calculated an integral of $\kappa_u(\ell_A)/[\bar{\kappa}_u(-\ell_A) + \kappa_u(\ell_A)]$ for each line ℓ_A of element A, then added all the integrals. For each $\kappa_u(\ell_A)$, GLAM used the detailed line profile. However, they evaluated $\bar{\kappa}_u(-\ell_A)$ (that is, the opacity at frequency u excluding the contribution of the line of interest, also called the background) in an approximate way. The u interval from 0 to 20 was separated into 4000 equal Δu intervals, and all contributions to $\bar{\kappa}_u(-\ell_A)$ within a given interval (including the remaining A lines and A continuum) were averaged. The exact value of $\bar{\kappa}_u(-\ell_A)$, the background, was then never calculated at one given frequency, but rather averaged within the interval Δu. Integration for each line ℓ_A was then performed by analytical or numerical means, assuming that the local background opacity *for that line*, $\bar{\kappa}_u(-\ell_A)$, was in fact *the* background opacity for all u.

The accuracy of this method is limited by the average nature of the background. To calculate the background (but not to calculate $\kappa_u(\ell_A)$), one assumes that each line with its center within a given interval is entirely within that interval, and that all lines have a square shape of width Δu. In the calculations of GLAM, the only exception was for hydrogen lines, which were calculated in detail and generally covered many intervals. The continua pose no problems as long as they do not vary too rapidly over Δu.

This method is partly motivated by the statistical nature of blends when energy levels are not measured but calculated, as is the case for OPAL and OP. Since we do not know the exact wavelength of each component of a blend, the effect of blends can only be evaluated in an average way. This method has the advantage of taking into account all lines of A as well as all lines of all elements included in the background. However, the averaging process becomes less accurate if the compromise average Δu used by GLAM becomes much larger or smaller than the physical line widths. Furthermore, the averaging process leaves no gap in line absorption unless there is no line over one interval Δu. The effects of these limitations on $g_R(A)$ are difficult to evaluate a priori.

LeBlanc et al. (1998) have compared $g_R(A)$ calculated using the averaging method of GLAM to $g_R(A)$ calculated using the opacity sampling method for a few values of (T, R) and for various compositions. They use the OP data available at Strasbourg and a detailed line profile for each line; the same physics (i.e., no correction) is applied in both cases. They perform calculations for the 4000 intervals of GLAM as well as opacity sampling for 4000, 10^4, 10^5, and 10^6 points in order to guarantee convergence to the correct value (preliminary results suggest that for $T > 10^5$ K, there are no significant differences produced by going from 10^5 to 10^6 frequencies). From their detailed comparison, we can conclude that GLAM underestimates g_R for $T \lesssim 10^6$ K. This is apparently caused by the averaging over each Δu, which leaves very few frequencies with no contribution from line absorption, so that there is no window where a large flux could be available for absorption by a line of interest. It appears to affect wings of moderate lines most, probably because such wings can be the main absorber at frequencies where no other line absorbs, a situation that occurs in opacity sampling calculations but not in calculations where an averaging of line contributions is done over Δu, as in GLAM. At higher temperatures ($T \gtrsim 10^6$ K), the GLAM approach overestimates g_R; it leaves many frequency intervals too transparent to radiative flux by concentrating the opacity from wide lines into narrower frequency intervals (of width Δu).

In practice, the radiative accelerations calculated by GLAM were also limited by the data available at Strasbourg. These turn out to be sufficient for CNO, but not for Fe (see also Seaton 1997).

The GLAM- and OPAL-based radiative accelerations are compared for C, N, and O in Figure 7. This figure illustrates the importance of the corrections discussed in § 3.1 as well as the generally satisfactory agreement between the two methods of calculation. The dotted curves represent the GLAM results, including corrections. The solid and dashed lines show the accelerations calculated by direct integration of OPAL spectra; for the solid line calculations, the resulting g_R were multiplied by pretabulated GLAM

[4] Following Seaton (1997), it can be argued that the $f_{\rm ion}$ should not be applied to autoionization resonances, which often dominate photoionization in nonhydrogenic cases.

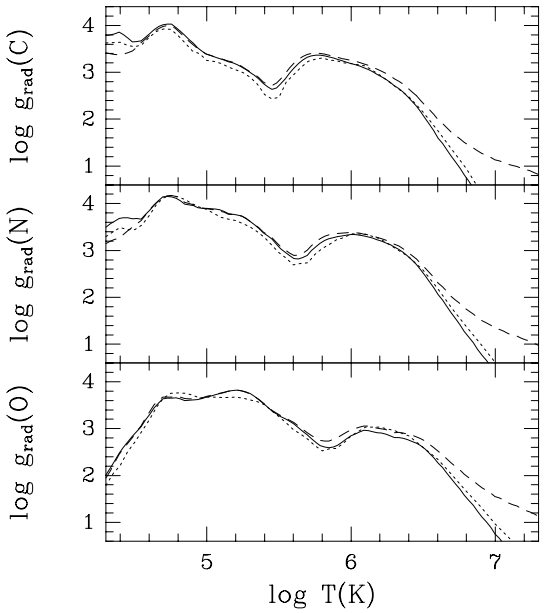

FIG. 7.—Radiative acceleration of C, N, and O, at $T_{\rm eff} = 10000$ K, log $R = -3.0$, for the abundance mix given in Table 1. Solid lines are OPAL plus corrections discussed in § 3 (corrections computed using OP atomic data); dashed lines are OPAL, uncorrected; dotted lines are GLAM, but using OPAL Rosseland mean opacities. Corrected values of g_R become negative at high temperature, due to $f_{\rm ion}$ corrections to photoionization.

correction factors[5] (similar to the $\Delta n = 0$ curves in Fig. 6). The GLAM results lie at most 0.2 dex below the corrected OPAL calculations. The two radiative accelerations agree very well for $6.0 < \log T < 6.5$, and the GLAM results become larger than the OPAL values above that range.

Factoring out physical corrections, as done here with OPAL data, is only approximate. In the GLAM calculations, corrections are incorporated before integrating over the spectrum and before averaging over ions; in the sampling calculations, they can only be applied at the very end. Only a small fraction of the difference seen between the solid and dotted curves in Figure 7 can come from this factorization (this was checked numerically for GLAM-type calculations).

4. EVOLUTIONARY EFFECTS: SELF-CONSISTENT CALCULATIONS

The radiative accelerations described above have been used for self-consistent evolution calculations. The calculations are described in detail and applied to solar models in Turcotte et al. (1998b), while the results for stars with M varying from 1.1 to 2.0 $M_\odot$ are given in Turcotte et al. (1998a). We use here some of their results for a 1.4 $M_\odot$ model to illustrate the effect of using self-consistent opacities and radiative accelerations in stellar models. The effect of radiative accelerations tends to increase with L_r/M_r. These have small effects in the Sun, but larger effects in more massive stars. We have chosen an intermediate-mass model, important for the Li gap (Boesgaard & Tripicco 1986; Michaud 1986), which we have been able to follow throughout its main-sequence life. As the stellar mass further increases, converging the models for their complete evolution becomes more difficult, as the larger radiative accelerations tend to cause numerical instabilities in the abundances, especially since the radiative accelerations have fluctuations that were not completely eliminated for the evolution calculations.

Figure 8 shows the effect of using monochromatic spectra to calculate Rosseland opacity in a 1.4 $M_\odot$ star evolved including the diffusion of He and metals. It is shown at $t = 0.86$ Gyr. The Rosseland opacity is increased by a factor of up to 2.5 compared to the Rosseland opacity interpolated in Y and Z in tables calculated using the same atomic data. Since $\log R \simeq -3$, $\log T \simeq 5.4$, and $\log g \simeq 5$ below the convection zone of this star, one can read from Figure 1 which elements are supported and which sink. The opacity change arises from an increase in the Fe abundance by a factor of 2.3, coupled to a decrease in Z by a factor of about 2. The decrease in Z comes mainly from the gravitational settling of CNO. When one interpolates in (Y, Z), the decrease of CNO dominates and reduces Z and the opacity. The increase in the Fe abundance has a small effect on Z, but a larger effect on the Rosseland opacity. Rosseland opacity tables for Fe-enhanced mixtures, together with already available tables for CO-enhanced mixtures (Iglesias & Rogers 1993) might sometime be a useful alternative to full-fledged opacity calculations in such circumstances. Iglesias & Rogers recently produced such Fe tables for a pulsation study of subdwarf B stars by Charpinet et al. (1997).

Turcotte et al. (1998a) give examples of the abundance evolution of various chemical elements and show that the opacity increase mentioned above leads to an increase in the depth of the convection zone by a factor of close to 2 in mass. This is caused by increased opacity from the increased Fe abundance and, to some extent, is an iron convection zone. One example of the abundance variation is given in Figure 9. Manganese has a much smaller effect on the stellar structure than Fe because of its smaller abundance. In this star, it has a g_R that is similar to that of Fe (not shown).

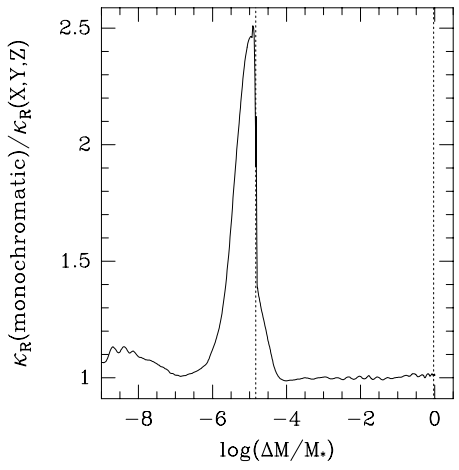

FIG. 8.—Ratio of the Rosseland opacity calculated from the monochromatic opacities of each species at the same time that the evolution proceeds to the Rosseland opacity in the OPAL 1996 tables. The local Y and Z values are continuously recalculated as evolution proceeds. Those values are used to interpolate in the tables. However, because X(Fe) increases while Z decreases for $\log \Delta M/M_* < -4$, the tables give opacities up to 2.5 times too small. The low-amplitude oscillations, seen mainly for $\log \Delta M/M_* > -4$, arise from interpolation differences in the two evaluations of the opacity. Dotted lines mark the star center and the bottom of the surface convection zone.

[5] The correction tables used give the ratio of the corrected to the uncorrected GLAM g_R's for each element at our standard chemical composition over a large temperature-density grid.

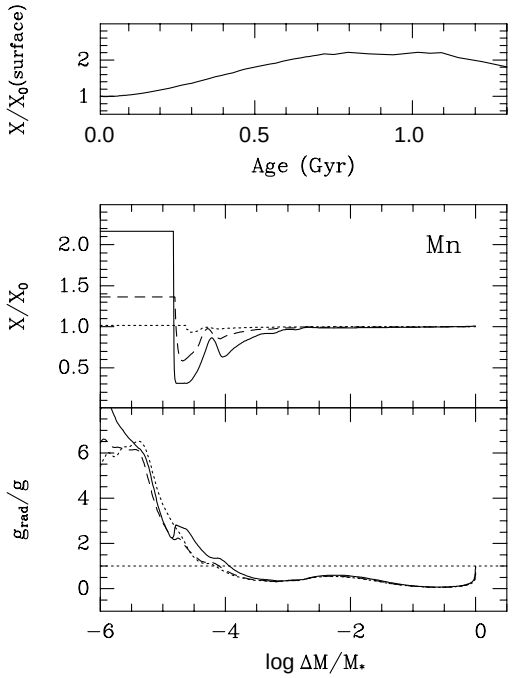

FIG. 9.—Time evolution of the abundance and radiative acceleration of Mn in a 1.4 $M_\odot$ model. Upper panel shows the time evolution of the abundance in the convection zone and atmosphere. Middle panel shows the profile of the Mn abundance within the star at $t = 0.07$ (*dotted line*), 0.30 (*dashed line*), and 0.86 (*solid line*) Gyr; the radiative acceleration is shown at the same times in the lower panel.

From the lower panel, one sees that g_R(Mn) is larger than gravity through a zone extending from the bottom of the convection zone ($\log \Delta M/M_* \simeq -5.2$) to $\log \Delta M/M_* = -4$. Approximately 1/3 of the Mn originally in that zone is concentrated in the convection zone by the time the star is 0.86 Gyr old. Manganese is also sinking toward the center throughout the region where $g_R(\mathrm{Mn}) < g$, leading to a local underabundance of Mn. The ratio $g_R(\mathrm{Mn})/g$, however, increases very close to the center and becomes equal to one at $0.02R_*$ from the center. This is caused by energy generation being more concentrated toward the center than the mass. This increase in g_R limits the abundance change of Mn close to the center to about 1% after 0.86 Gyr.

The radiative accelerations based on the 10^4 point opacity sampling of OPAL can conveniently be used to evolve stellar models that include the diffusion of all important species contributing significantly to the opacity. The g_R, however, become progressively less accurate as temperatures become smaller than 10^5 K. This allows a calculation of the effects of atomic diffusion on stellar evolution in so far as stellar structure is not very sensitive to surface phenomena. It does not allow calculation of the effects of diffusion on the photospheric anomalies observed in HgMn stars, or even in the warmer of the AmFm stars. These require a different treatment. For these, one would ideally use opacity sampling with a 10 times finer grid, which would likely be sufficient for most cases of interest. Until this becomes available, the preferred approach is to use opacity sampling as presented here to calculate Rosseland opacities, taking into account the effect of abundance variations. For the radiative accelerations at $T \leq 10^5$ K, the results from opacity sampling could be used to calibrate approximate formulas, such as those of Alecian & Artru (1990) and Alecian (1994), which would then filter the random variations caused by insufficient sampling. Alternatively, the radiative accelerations could be taken from tables such as those of Seaton (1997), which do not at present include the effect of abundance variations (other than those of the element for which one calculates g_R), or those of GLAM.

This research was partially supported at the Université de Montréal by NSERC. F. L. would like to thank the Faculté des Études Supérieures et de la Recherche de l'Université de Moncton for funding. Work by F. J. R. and C. A. I. was performed under the auspices of the Department of Energy at Lawrence Livermore National Laboratory under contract W-7405-Eng-48.

REFERENCES

Alecian, G. 1994, A&A, 289, 885
Alecian, G., & Artru, M.-C. 1990, A&A, 234, 323
Boesgaard, A. M., & Tripicco, M. J. 1986, ApJ, 302, L49
Chapman, S., & Cowling, T. G. 1970, The Mathematical Theory of Non-Uniform Gases (3rd ed; Cambridge: Cambridge Univ. Press)
Charpinet, S., Fontaine, G., Brassard, P., Chayer, P., Rogers, F. J., Iglesias, C., & Dorman, B. 1997, ApJ, 483, L123
Chayer, P., Fontaine, G., & Wesemael, F. 1995, ApJS, 99, 189
Gonzalez, J.-F., Artru, M.-C., & Michaud, G. 1995a, A&A, 302, 788
Gonzalez, J.-F., LeBlanc, F., Artru, M.-C., & Michaud, G. 1995b, A&A, 297, 223 (GLAM)
Iglesias, C. A., & Rogers, F. J. 1993, ApJ, 412, 752
———. 1995, ApJ, 443, 460
———. 1996, ApJ, 464, 943
LeBlanc, F., & Michaud, G. 1995, A&A, 303, 166
LeBlanc, F., Michaud, G., & Richer, J. 1998, in preparation
Massacrier, G. 1996, A&A, 309, 979
Massacrier, G., & El-Murr, K. 1996, A&A, 312L, 25
Michaud, G. 1970, ApJ, 160, 641
Michaud, G. 1986, ApJ, 302, 650
Michaud, G., Charland, Y., Vauclair, S., & Vauclair, G. 1976, ApJ, 210, 447
Michaud, G., Martel, A., & Ratel, A. 1978, ApJ, 226, 483
Michaud, G., Montmerle, T., Cox, A. N., Magee, N. H., Hodson, S. W., & Martel, A. 1979, ApJ, 234, 206
Michaud, G., Vauclair, G., & Vauclair, S. 1983, ApJ, 267, 256
Richer, J., Michaud, G., & Massacrier, G. 1997, A&A, 317, 968
Rogers, F. J., & Iglesias, C. A. 1992a, ApJS, 79, 507
———. 1992b, ApJ, 401, 361
Seaton, M. J. 1995, J. Phys. B, 28, 3185
———. 1997, MNRAS, 289, 700
Seaton, M. J., Yan, Y., Mihalas, D., & Pradhan, A. K. 1994, MNRAS, 266, 805
Sommerfeld, A., & Schurr, G. 1930, Ann. Phys. (Leipzig), 4, 409
Schurr, G. 1930, Ann. Phys. (Leipzig), 4, 433
Turcotte, S., Richer, J., & Michaud, G. 1998a, in preparation
Turcotte, S., Richer, J., Michaud, G., Iglesias, C., & Rogers, F. 1998b, in preparation
Vauclair, S., & Vauclair, G. 1982, ARA&A, 20, 37